

Attractive and Repulsive Electrostatic Forces between Positively Charged Latex Particles in the Presence of Anionic Linear Polyelectrolytes

Ionel Popa,[‡] Graeme Gillies,[§] Georg Papastavrou,^{||} and Michal Borkovec*

Department of Inorganic, Analytical, and Applied Chemistry, University of Geneva, Sciences II, 30, Quai Ernest-Ansermet, 1211 Geneva 4, Switzerland

Received: December 3, 2009; Revised Manuscript Received: January 27, 2010

The interaction forces between individual positively charged amidine functionalized latex particles with adsorbed negatively charged sodium poly(styrene sulfonate) were studied with the colloidal probe technique based on atomic force microscopy (AFM). When the polymer dose is progressively increased, the strength of the repulsive force between the particles decreases as the charge neutralization point is approached, then increases again due to overcharging, and finally reaches a plateau. Surface potentials obtained from fits of the force profiles to Poisson–Boltzmann theory agree well with potentials measured with electrophoresis. Close to the charge neutralization point, attractive forces exceeding van der Waals interactions are found. These attractive forces increase in strength with increasing molecular mass of the polymer and decreasing ionic strength. These attractive interactions are of electrostatic origin and result from lateral patch–charge heterogeneities within the adsorbed polyelectrolyte layer. The measured forces are shown to be in semiquantitative agreement with model calculations based on charge distributions with square lattice symmetry.

Introduction

Colloidal stability of aqueous particle dispersions is relevant in natural systems (e.g., self-cleaning capacity of lakes, transport of particles in a subsurface),^{1,2} and industrial applications (e.g., papermaking, water–water treatment, formulation of paints).^{3–5} Particles in aqueous suspensions normally carry an electric surface charge due to ionic substitution or charged surface groups. The classical theory of Derjaguin, Landau, Verwey, and Overbeek (DLVO) asserts that dispersions of such particles are stable at low salt concentrations due to the repulsive electrostatic forces caused by the overlap of the diffuse layers.⁶ Addition of salt destabilizes such suspensions, whereby aggregation is induced by attractive van der Waals forces and screening of repulsive electrostatic interactions by salt. This situation is summarized in Figure 1.

An alternative way to destabilize charged colloidal suspensions is by adding oppositely charged polyelectrolytes.^{3,4} Various cationic polyelectrolytes have been used in this context, since colloidal particles in industrial applications are often negatively charged (e.g., silicates, clays, cellulose). Positively charged particles can be similarly destabilized with anionic polyelectrolytes. This situation is important in natural waters, where the stability of positively charged iron oxide particles is controlled by humic acids or alginates, both of which are naturally occurring anionic polyelectrolytes.^{7–9}

Polyelectrolytes control suspension stability by their strong affinity to the oppositely charged particle surface, which leads to charge neutralization and subsequent charge reversal (i.e., overcharging).^{10–16} DLVO theory predicts that the suspension

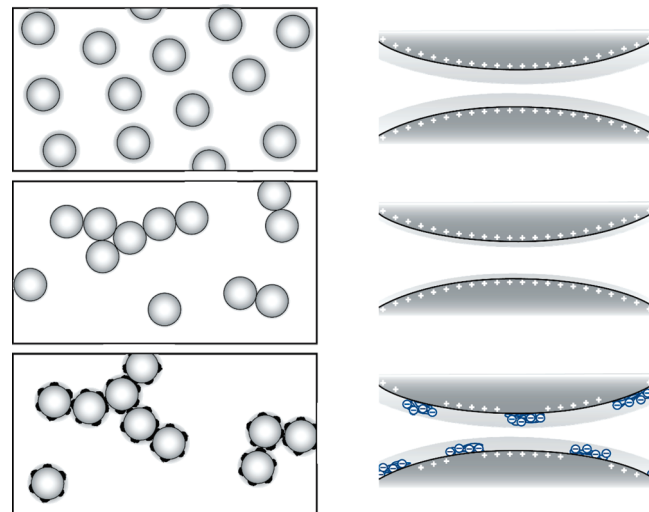


Figure 1. Scheme of a colloidal dispersion of charged particles in low salt (top left), aggregation induced by salt (middle left), and aggregation by adsorbed oppositely charged polyelectrolyte (lower left). The schemes in the right column illustrate the corresponding interaction forces.

is unstable near the isoelectric point (IEP) where the interactions between the particles are dominated by attractive van der Waals forces. Away from the IEP, electrostatic repulsion due to diffuse layer overlap becomes operational and the suspension becomes stable.

While this simple DLVO picture captures the main features in the stability of polyelectrolyte-particle systems, numerous authors have argued that additional attractive interactions are operational.^{10,12,15} The most obvious manifestation of these non-DLVO forces is that aggregation can be more rapid in the presence of a polyelectrolyte than in the presence of salt. Two explanations concerning the origin of additional attractions have been put forward.¹⁶ The first one proposes that the additional

* Corresponding author. E-mail: michal.borkovec@unige.ch. Phone: +41 22 379 6405. Fax: +41 22 379 6069.

[‡] Current address: Department of Biological Sciences, Columbia University, New York, 10027.

[§] Current address: Adolphe Merkle Institute, University of Fribourg, CH-1723 Marly 1, Switzerland.

^{||} Current address: Physical Chemistry II, University of Bayreuth, Bayreuth, Germany.

attraction originates from polymer strands bridging the two surfaces.^{4,17,18} The second explanation suggests that attractive interactions are electrostatic in origin, and result from the patchwise heterogeneous charge distribution due to the adsorbing of the highly charged polyelectrolyte to an oppositely charged surface.^{10,14,19,20}

In order to clarify the origin of these attractive non-DLVO forces, direct force measurements were carried out in systems containing oppositely charged polyelectrolytes with the surface forces apparatus, a colloidal probe based on an atomic force microscope (AFM), or similar techniques.^{7,18,21–27} These studies confirmed the existence of repulsive DLVO forces due to diffuse layer overlap well above the IEP, where the adsorbed amount of the polyelectrolyte is high. The interesting region near the IEP could be explored by direct force measurements only with difficulties. Nevertheless, the existence of attractive forces exceeding van der Waals forces was reported.^{18,21} However, these forces occurred only in a transient-like fashion, and therefore their origin could not be pinpointed.

With a novel multiparticle colloidal probe technique, we have recently measured accurate force profiles between positively charged amidine latex particles with adsorbed anionic poly(styrene sulfonate) (PSS) at the IEP.²⁸ This study concluded that attractive non-DLVO forces are due to patch–charge interactions and that bridging forces are negligible. The conclusion was mainly based on the following observations. First, a pronounced ionic strength dependence of these attractive forces suggests their electrostatic origin. Second, the number of bridging events could be quantified, but they were shown to be extremely rare and not correlated to the strength of the forces upon approach. Third, analogous findings were made in a system with negatively charged sulfate latex particles with adsorbed cationic poly(amido amine) (PAMAM) dendrimers, where the role of bridging forces must be absent or strongly reduced as a result of the conformational constraints implied by the dendrimer architecture.²⁹ Finally, colloidal stability determined by light scattering in both systems followed a very similar pattern.^{13,15} Since the charges are inverted in these two systems, their congruence clearly suggests that the interactions are governed by electrostatics.

The present article analyzes the previously mentioned direct force measurements between positively charged amidine latex particles with adsorbed anionic PSS in terms of different electrostatic models. We quantify the strength of the repulsive DLVO interactions in terms of an effective charge. Moreover, attractive non-DLVO forces are shown to be semiquantitatively consistent with a patch–charge interaction model proposed previously.^{30,31}

Experimental Section

Materials. Sodium PSS with molecular masses of 29, 323, and 2260 kg/mol and a polydispersity index smaller than 1.2 was purchased from Polymer Standards (Germany). Amidine-terminated surfactant-free polystyrene latex particles were obtained as an aqueous suspension from Interfacial Dynamic Corporation (Portland, OR). The diameter of the particles was 3.3 μm , and the polydispersity index was 8.7%, as determined by transmission electron microscopy by the manufacturer. A charge density of +350 mC/m² obtained by conductometry was also reported. The concentration of the stock suspension was confirmed with total organic carbon analysis (TOC-V). Before use, the latex particles were dialyzed for 6 h in a Millipore ultrafiltration apparatus. The final particle concentration was determined by comparing the dialyzed samples with nondialyzed

ones with static light scattering and TOC. All the measurements were carried out at pH 4.0, which was adjusted with HCl. The ionic strength was controlled with KCl. All solutions were prepared with water purified in a Milli-Q Millipore system. All experiments were carried out at room temperature near 22 °C.

Electrophoresis. The electrophoretic mobilities of the latex particles in suspension were determined with laser Doppler velocimetry (Zetasizer 2000, Malvern Instruments, U.K.) and video microscopy (Zetacompact, CAD Instruments, France). The electric fields used were in the range of 75–150 V/cm. Both techniques yielded the same results within 10%. The electrophoretic mobilities were converted into surface potentials with the standard electrokinetic model.³² Electrophoresis was further used for quality control, and only samples where all the particles were moving in the same direction were further analyzed with the colloidal probe technique.

AFM Imaging. Images were obtained with a Nanoscope IIIa AFM (Vecco, Santa Barbara), operated in air and in tapping mode. To image adsorbed PSS on colloidal particles, the particles were first left to react overnight with the polymer in suspension in an electrolyte solution of pH 4.0 and an ionic strength of 1.1 mM. Subsequently, the particles were deposited on a Millipore membrane with a pore size of 1.2 μm . The membrane was washed with water and dried under vacuum. Surfaces of the immobilized particles were imaged with standard tapping-mode cantilevers (OMLC-AC160TS-W2, Olympus).

AFM Force Measurements. The colloidal probe technique was used to measure the interaction forces between latex particles. The AFM (MFP-3D, Asylum Research) was mounted on an inverted optical microscope (Olympus IX 70). The glass plate of the AFM fluid-cell was cleaned for 40 min at 80 °C with piranha solution, which is a mixture of H₂SO₄ 98% and H₂O₂ 30% in a ratio of 3:1, and rinsed extensively with water. Subsequently, the surfaces were treated for 20 min in an air-plasma cleaner and silanized with hexamethyldisilazane (Sigma-Aldrich) for 2 h in an airtight container under vacuum. The silanization process was controlled through the contact angle of water, which had to exceed 30°. The cantilevers were cleaned in an air-plasma cleaner for 20 min and silanized in the same way.

The particle suspension was mixed with the corresponding amount of PSS at pH 4.0 and an ionic strength of 1.1 mM adjusted with KCl and left to deposit at the surface of the fluid-cell under vacuum for about 6 h. Subsequently, the suspension was replaced with the pure electrolyte solution, which was previously degassed for at least 2 h with a Gastorr degasser operating at 100 MPa. The electrolyte solution, in which the force measurements were carried out, had eventually a different ionic strength than the one used in the adsorption process. A colloidal particle was firmly attached to the tip-less cantilever by repeatedly pressing the particle to the substrate and thereby rolling it. Finally, this particle was centered with respect to another particle immobilized at the surface through the resulting interference pattern observed in the optical microscope. The alignment has a lateral precision of about 0.2 μm .

The interaction forces were measured by approaching the probe vertically to the particle immobilized at the surface until the constant compliance region was reached. Upon retraction of the cantilever, a jump-out was observed. The deflection of the cantilever was monitored by the reflection of a laser beam. The interaction forces were obtained by averaging about 100 approach and retraction cycles, which were accumulated with a frequency of 0.5 Hz and approach velocities of 400–800 nm/s. After a measurement sequence, the particle used was detached

and another particle was attached to the cantilever. In this fashion, different pairs of particles were measured for the same samples.

The zero separation was determined from the constant compliance region with a precision of about 0.2 nm. The cantilever spring constants were measured with three independent methods.^{33–35} These results agreed typically within 20% and the average of the three measured values was used to calculate the forces. The force constants of the cantilevers were between 0.04 and 0.3 N/m. The stiffer cantilevers are needed for the measurement of the attractive force profiles. The measured forces were finally normalized with the effective radius $R_{\text{eff}} = R_1 R_2 / (R_1 + R_2)$ where R_1 and R_2 are the radii of the two interacting spheres. These radii were determined with an accuracy of about 0.2 μm by optical microscopy.

Forces between colloidal particles remained constant over periods of several hours, including the particles with adsorbed PSS. The constancy of the forces in the latter systems indicated that the adsorption of PSS is basically irreversible, and that no desorption takes place over substantial periods of time, even at the highest ionic strengths investigated. A similar conclusion can be reached from the independency of the electrophoretic mobility on the particle concentration in a similar system.¹⁵

Results and Discussion

The present article discusses interaction forces between individual positively charged latex particles of 3.3 μm in diameter with adsorbed anionic polyelectrolyte PSS in aqueous electrolyte solutions. Since these direct force measurements are carried out in suspensions and in presence of a large number of immobilized particles, the resulting large surface area exceeding 1 m^2 allows an accurate control the polyelectrolyte dose. The particles are directly mounted to silanized substrates in the electrolyte solution. Thereby, one avoids the problematic drying-rewetting step, which is common in the preparation of colloidal probes and often leads to the formation of microscopic bubbles at the particle surface.

AFM Imaging. A typical image of the surface of the latex particles is shown in Figure 2a. The image reveals no particular features and is quite smooth with a mean square roughness of about 0.4 nm. Adsorbed PSS on the latex particles can be only distinguished in AFM phase images shown in Figure 2b,c. At the lower dose of 0.9 mg/g, one recognizes that the adsorbed polyelectrolyte forms a heterogeneous layer made of irregular patchy structures. We suspect that at this dose the polyelectrolyte adsorbs quantitatively. At a higher PSS dose of 1.3 mg/g, the layer becomes denser, but remains laterally heterogeneous. This dose leads to a saturated adsorption layer, and the excess polyelectrolyte remains dissolved in solution. Therefore, the adsorbed amount stays constant even when the polyelectrolyte dose is increased further. From the AFM images, we roughly estimate a surface coverage of around 0.35 at the IEP and 0.5 in the saturated layer. These observations indicate that the adsorbed polyelectrolyte layers are laterally heterogeneous, even in their saturated state. This lateral heterogeneity can be explained through the repulsive electrostatic forces between the charged adsorbing polyelectrolyte chains.

Repulsive Forces. The bare latex particles are positively charged and interaction forces are dominated by electrostatic repulsion due to diffuse layer overlap. Typical force profiles measured in an electrolyte solution of pH 4.0 and an ionic strength of 1.1 mM are shown in Figure 3. These forces are consistent with DLVO theory and can be quantified with the classical Poisson–Boltzmann (PB) model.⁶ At larger distances,

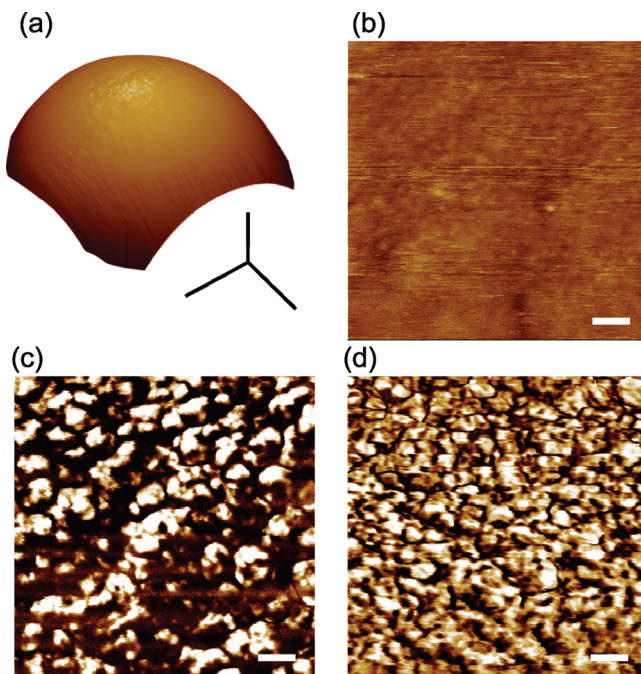


Figure 2. AFM images of amidine latex particle. (a) Three-dimensional AFM image of the bare amidine latex particle and (b) the flattened image. Flattened images of particles with adsorbed PSS of 2260 kg/mol (c) at IEP and (d) at saturation. The white scale bars in panel a correspond to 1 μm , while those in b–d correspond to 50 nm.

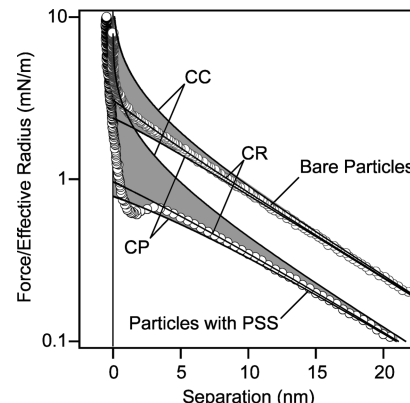


Figure 3. Force profiles between amidine latex particles at pH 4.0 and an ionic strength of 1.1 mM in KCl without and with adsorbed PSS at saturation. The solid lines are fits based on PB theory with CR boundary condition. The gray area indicates the regime between CC and CP boundary conditions.

the forces decay exponentially. Their amplitude is given by the diffuse layer potential ψ_d , and the decay length is given by the Debye length κ^{-1} . The latter parameter can be expressed as

$$\kappa^2 = \frac{2e^2 N_A I}{\varepsilon \varepsilon_0 k T} \quad (1)$$

where e is the elementary charge, N_A is Avocadro's number, I is the ionic strength, $\varepsilon \varepsilon_0$ is the dielectric permittivity of water, k is the Boltzmann constant, and T is the absolute temperature. For the data shown in Figure 3 for the bare particles, one finds a decay length of about 7.9 nm, which agrees quite well with the Debye length of $\kappa^{-1} \approx 9.2$ nm calculated from the ionic strength of the solution. The diffuse layer potential turns out to

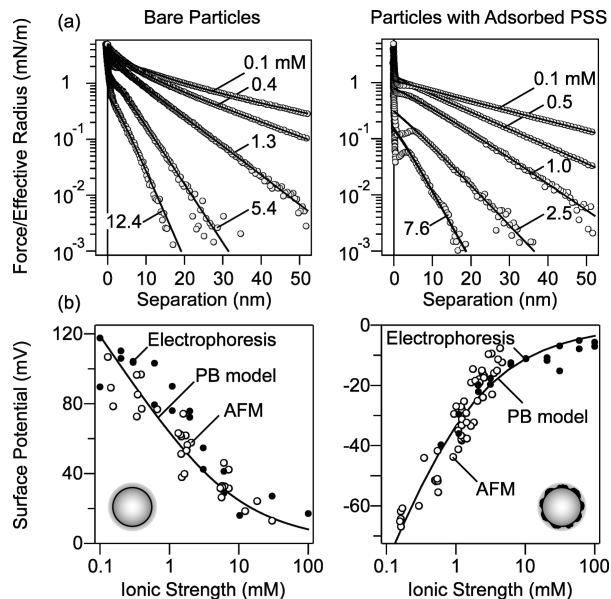


Figure 4. Force profiles between bare amidine latex particles (left) are compared with the same particles with a saturated layer of PSS with a molecular mass of 2260 kg/mol (right) at pH 4.0 and different ionic strengths. (a) Force profiles normalized to the effective radius of the particles as a function of the separation. Solid lines are fits of PB theory with CR condition. (b) Surface potentials obtained from the AFM experiment (open symbols) are compared with electrophoresis data (full symbols). Solid lines are fits to PB theory.

be $\psi_d = 61.7$ mV, whereby the positive sign is obtained from the electrophoresis data independently.

While the classical constant charge (CC) and constant potential (CP) boundary conditions agree poorly with the experimental data at smaller separation distances, a much better description can be obtained with the constant regulation (CR) boundary condition.³⁶ This approximation introduces an adjustable regulation parameter $p \leq 1$, whereby one recovers the classical conditions for CC with $p = 1$ and CP with $p = 0$. The regulation parameter can even become negative, whereby the force is even weaker than in the CP case.³⁷ For the data shown in Figure 3, one finds $p \approx 0.27$. Since this number is substantially smaller than unity, we conclude that that charge regulation is important indeed.

Similar interaction force profiles are found when PSS of a molecular mass of 2260 kg/mol is adsorbed to the particles in an KCl electrolyte solution of pH 4.0 and an ionic strength of 1.1 mM at a dose of 4.9 mg/g. These conditions lead to a saturated adsorption layer. The forces are measured in the same electrolyte solution but in the absence of PSS. Since the force profiles remain constant over periods of several hours, the adsorption is irreversible and no desorption occurs. The forces can be again rationalized with the PB theory with CR boundary conditions. The resulting decay length of 8.1 nm agrees well with the expected Debye length of $\kappa^{-1} \approx 9.2$ nm. The diffuse layer potential turns out to be $\psi_d = -38.2$ mV and the regulation parameter is $p \approx 0.11$. Effects of charge regulation are important for the description of the force profiles at small separations.

Figure 4a compares the ionic strength dependence of the force profiles between the bare amidine particles and the same particles with a saturated layer of PSS of 2260 kg/mol, which was adsorbed at pH 4.0 and an ionic strength of 1.1 mM. In both cases, the forces are repulsive and their range decreases with increasing ionic strength. At larger distances, the forces can be fitted very well to the PB model with CR condition. The measured decay lengths agree with the expected Debye

length within 15%. The regulation parameter is in the range 0.35 ± 0.04 for the bare particles and 0.32 ± 0.02 for the particles with adsorbed PSS. This parameter increases slightly with increasing ionic strength. At small separation distances, strong repulsive forces set it. The small range of these forces suggests very thin adsorbed layers, which is in contrast to longer range repulsive interactions observed for grafted polyelectrolytes or those adsorbed at high ionic strengths.^{24,27}

The surface potentials obtained from the fits of the force profiles are compared with the ζ -potentials calculated from the electrophoretic mobility in Figure 4b. Good agreement between these two independent methods is found. The signs of the potentials obtained from the force profiles were assigned based on the electrophoresis. PB theory relates the diffuse layer potential ψ_d to the surface charge density σ with the Gouy–Chapman equation

$$\psi_d = \frac{2kT}{e} \operatorname{asinh}\left(\frac{e\sigma}{2kT\epsilon\epsilon_0\kappa}\right) \quad (2)$$

The fits of the ionic strength dependence of the surface potentials with this relation are shown in Figure 4b. For the bare particles, one finds a surface charge density of 5.9 ± 0.3 mC/m². This charge density is substantially smaller than the conductometric value of 350 mC/m². We suspect that this substantial discrepancy originates from the specific adsorption of chloride ions from the electrolyte solution. The same procedure yields a charge density of -2.6 ± 0.1 mC/m² for the same particles with a saturated layer of adsorbed PSS. The good fit of the latter data further confirms that the amount of the adsorbed PSS remains constant and no desorption takes place within the experimental time scale.

Charge Reversal. Figure 5 shows the force profiles between the latex particles as a function of the polyelectrolyte dose. PSS of 2260 kg/mol was adsorbed in a KCl electrolyte solution of pH 4.0 and an ionic strength of 1.1 mM. Forces were measured in the same electrolyte solution in the absence of PSS. No desorption of PSS takes place under these conditions, as was inferred from the constancy of the force profiles with time. The bare particles show strong repulsion due to overlap of diffuse layers. As the PSS dose is increased, the adsorbed polyelectrolyte reduces the overall surface charge density, and the strength of the repulsion decreases. Figure 5a illustrates this trend. At the same time, a short-range attraction is found. At a dose of 0.9 mg/g, the particle surface charge is precisely neutralized by the adsorbed polyelectrolyte and no repulsive forces are observed. At this point, the interaction is completely dominated by the short-range attraction. This attraction is stronger than the van der Waals interaction and originates from the electrostatic interactions between patch–charge heterogeneities induced by the adsorbed negative PSS on the positively charged particle surface. These forces will be discussed in detail below.

By increasing the polyelectrolyte dose further, the forces between the particles become repulsive again (see Figure 5b). The repulsion is caused by the overlap of the diffuse layers. These diffuse layers form since the adsorbed PSS leads to the buildup of a negative surface charge. For doses of 1.3 mg/g and above, the repulsive force remains constant. This constancy originates from the formation of a saturated adsorbed layer. The strength of the short-ranged attraction decreases as one approaches the saturation plateau.

The diffuse layer potential was calculated for different pairs of particles by fitting the repulsive part of the force curves to

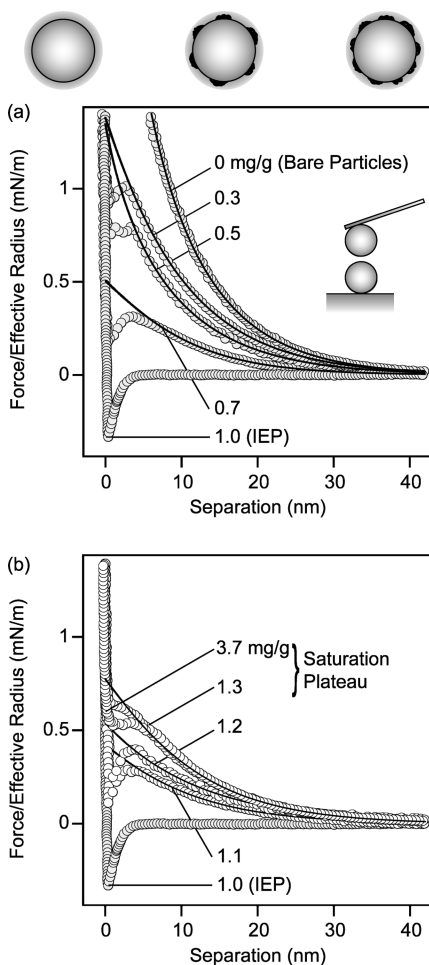


Figure 5. Force profiles as a function of separation between amidine latex particles with different doses of PSS 2260 kg/mol in 1 mM KCl electrolyte solution at pH 4.0. The solid lines are best fits to PB theory with CR condition. (a) Below and at IEP and (b) at IEP and above.

the PB theory with CR conditions. The measured decay lengths agreed with the estimated Debye length within 15%. The regulation parameter was in the range 0.31 ± 0.02 and did not show any clear trends with the polymer dose. The fitted diffuse layer surface potentials are shown as a function of the PSS dose in Figure 6a and they are compared with the ζ -potentials obtained from electrophoresis. The latter technique was also used to assign the sign of the diffuse layer potential obtained from AFM. Potentials measured with the two different techniques agree well. With increasing PSS dose, the potential decreases, and vanishes at the IEP, which is characterized by a dose of 0.9 ± 0.1 mg/g. When the dose is increased further, the potential becomes negative as a result of further adsorption of the negatively charged PSS. For doses exceeding 1.3 ± 0.1 mg/g, the measured repulsive forces and the ζ -potentials remain approximately constant. This constancy indicates that a saturated adsorbed layer is formed. The good agreement between the surface potentials measured with the two different techniques further demonstrates that no desorption of PSS takes place.

Results of further measurements are shown for PSS of lower molecular masses, namely for 29 kg/mol and 323 kg/mol. These findings are very similar to the results for PSS of high molecular mass. The surface potential is independent of the molecular mass of the PSS, suggesting that the charging behavior is dictated by the individual PSS segments. This observation is consistent with previous electrophoretic mobility measurements, which demonstrate that the IEP of amidine latex particles with adsorbed

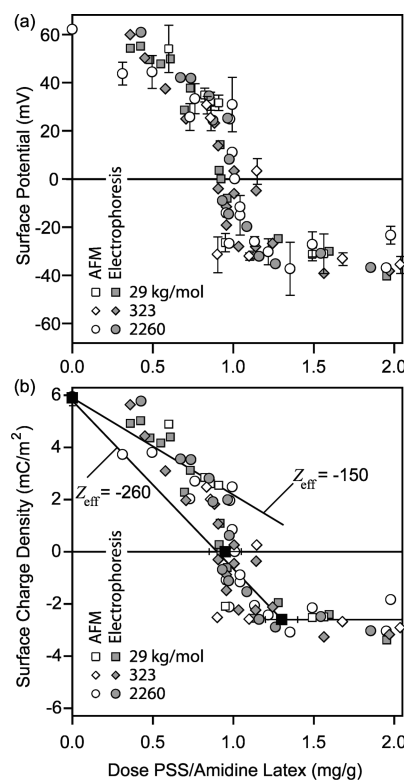


Figure 6. Surface potentials of amidine latex particles as a function of the dose of PSS for different molecular mass measured at pH 4.0 and ionic strength of 1.1 mM in an KCl electrolyte. The results obtained with AFM (open symbols) are compared with electrophoretic mobility data (gray symbols). (a) Surface potential and (b) the surface charge neutralizing the diffuse layer. The solid symbols (■) originate from independent measurements.

PSS is independent of the molecular mass.¹⁵ This lack of molecular mass dependence further confirms that PSS adsorbs in flat conformation.

Effective Charge and Charging Ratio. The surface charge neutralizing the diffuse layer can be obtained from the surface potentials with the Gouy–Chapman relation (eq 2). The results shown in Figure 6b illustrate that the surface charge decreases with increasing PSS doses and saturates at the adsorption plateau. The simplest way to interpret this decrease is to assume that each adsorbed polyelectrolyte chain contributes to the resulting charge in an additive fashion, namely,³⁸

$$\sigma = \sigma_0 + eZ_{\text{eff}}\Gamma \quad (3)$$

where Z_{eff} denotes the effective charge of the adsorbed PSS molecule in units of the elementary charge e , Γ is the number density of the adsorbed PSS, and σ_0 is the surface charge density. As shown in the left part of Figure 4a, $\sigma_0 \approx 5.9 \text{ mC/m}^2$ was found for the bare amidine latex particles with the AFM.

The effective charge can be precisely estimated at two doses: at the IEP, where $\sigma = 0$, and at adsorption plateau, where $\sigma = -2.6 \text{ mC/m}^2$ as shown in Figure 4b. In both cases, the effective charge of PSS turns out to be the same within experimental error, namely $Z_{\text{eff}} \approx -260$. Since these two estimates coincide, one might be inclined to think that the effective charge of PSS remains constant as the adsorbed amount increases. This case is illustrated with the straight line in Figure 6b. However, the experimental data indicate that the situation is more complicated. The surface charge density decreases much more weakly at low polymer dose, and this behavior can be interpreted with an

TABLE 1: Bare and Effective Charge of PSS

molecular mass ^a (kg/mol)	bare charge ^b Z	effective charge ^c Z _{eff}
29	-141	-3.3
323	-1568	-37
2260	-10 971	-260

^a Data provided by the manufacturer. ^b Calculated from the molecular mass. ^c Evaluated from the IEP.

effective charge of lower magnitude, around $Z_{\text{eff}} \approx -150$. Below IEP, the surface charge density decreases abruptly, and then it decreases approximately linearly as one expects for $Z_{\text{eff}} \approx -260$. For lower molecular masses, the effective charges are summarized in Table 1. Their values are lower in magnitude, but the overall behavior remains similar. In all cases, the effective charges of the PSS molecules correspond about to 2% of their bare charges.

We suspect that the abrupt transition in Figure 6b signals the onset of the lateral overlap between the diffuse layers around individual adsorbed PSS chains. At low adsorbed amount, the PSS chains adsorbed at the surface will be well separated. Their charge will be neutralized by diffuse layers, which form around each chain, leading to a strongly heterogeneous lateral charge distribution. As the adsorbed amount increases, these diffuse layers start to overlap and the lateral charge distribution becomes more homogeneous. Very similar behavior was observed with adsorbed cationic PAMAM dendrimers on negatively charged sulfate latex particles.³⁹ With increasing adsorbed amount, the effective charge remained low initially and increased abruptly to a higher value. This behavior was equally interpreted with a transition between a heterogeneous lateral charge distribution to a more homogeneous one at higher adsorbed amount. For PAMAM dendrimers, this transition is located after the IEP, leading to two markedly different values of the effective charge at IEP and at the saturation plateau. In the present situation, however, this transition occurs below the IEP. This difference is probably related to the larger lateral extent of adsorbed linear PSS chains in comparison to the highly branched and compact PAMAM dendrimers. This behavior might be equally related to the fact that the position of the IEP strongly depends on the molecular mass of the dendrimers, while no such dependence is observed here.

The presently reported effective charges are substantially smaller than the bare charge of the individual PSS chains (see Table 1). This difference suggests that the largest part of this charge is neutralized by the opposite surface charge of the latex particles. To make a quantitative comparison, let us consider the charging ratio, which denotes the ratio between the bare charge of adsorbed PSS chains and the bare surface charge of the particle.¹⁴ These quantities can be obtained from the chemical structure or conductometry. In the present system, we find a charging ratio of 0.7 ± 0.1 at IEP. This charging ratio compares well to the value of 1.6 reported for smaller amidine latex particles.¹⁵ The latter quantity was found to be independent of the ionic strength. These values indicate that the charge neutralization is close to stoichiometric, and that basically every charge of the PSS is neutralized by a charge on the particle surface. This observation suggests that small salt ions play only a minor role in the overall charge balance of the adsorbed layer. However, these ions seem to be relevant in the charge balance of the diffuse layer.

Attractive Forces. Figure 7 summarizes the measured attractive forces at the IEP. PSS was adsorbed in a KCl electrolyte solution at pH 4.0 and an ionic strength of 1.1 mM.

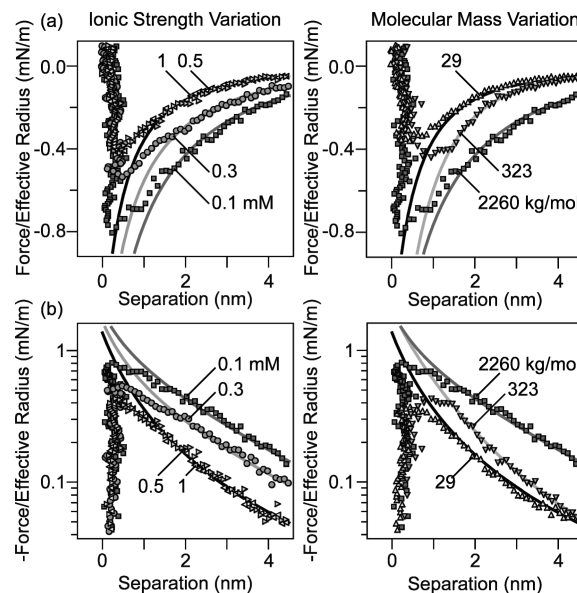


Figure 7. Attractive force profiles between amidine latex particles neutralized with adsorbed PSS at the IEP. Solid lines are best fits with eq 4. Comparison of different ionic strengths for molecular mass of 2260 kg/mol (left) and different molecular mass at an ionic strength of 0.1 mM (right). (a) Linear and (b) semilogarithmic representation of the negative force.

Forces were measured in electrolyte solutions without PSS at appropriate ionic strengths. One observes that attractions become stronger with decreasing ionic strength and with increasing molecular mass. Due to this dependence, these forces cannot originate from van der Waals interactions alone, and an additional attractive non-DLVO force must be present. We suppose that its dependence is exponential, and fit the observed force curves to the expression

$$\frac{F}{R_{\text{eff}}} = -\frac{H}{6} \cdot \frac{1}{(h + \delta)^2} - Ae^{-qh} \quad (4)$$

where h is the separation distance. The first term corresponds to the van der Waals interaction, where H is the Hamaker constant and δ is the displacement of the plane of origin with respect to the contact plane. The second term represents the additional exponential attractive force, where $A > 0$ is its amplitude and q^{-1} its range. Force profiles measured close to the IEP were also included in the analysis and fitted to eq 4 whereby an additional repulsive exponential force was added. Since the latter force originates from diffuse layer overlap, its range is given by the Debye length and its amplitude is adjusted. The attractive force was extracted by subtracting the fitted repulsive part. This procedure yielded consistent data with forces measured at IEP at the same conditions, and a larger number of attractive force profiles could be analyzed in this way. The resulting fits to eq 4 are shown as solid lines in Figure 7.

Forces at ionic strengths greater than or equal to 0.5 mM and for molecular masses less than or equal to 29 kg/mol are basically indistinguishable from the van der Waals force expected for this system. The forces are fitted with an expected value of $H = 9.0 \times 10^{-21}$ J for polystyrene.⁴⁰ The displacement of the plane of origin turns out to be $\delta = 1.1$ nm, which corresponds to a gap between the surfaces. These parameters were kept constant for all fits. This displacement is probably related to surface roughness of the latex particle, as this number corresponds quite well to the double of the mean square

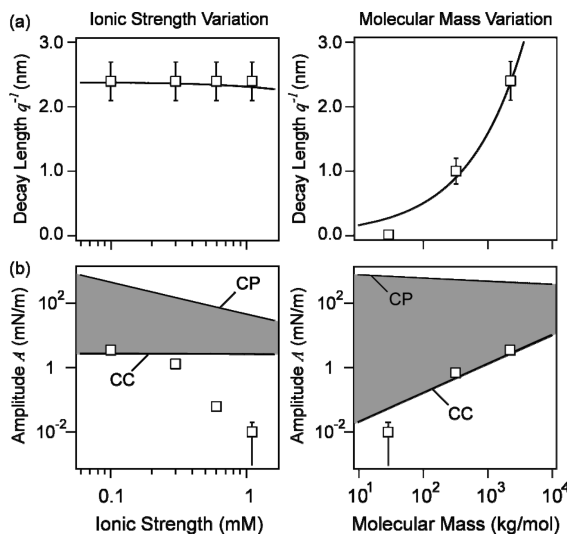


Figure 8. Parameters of additional exponential attractive force between amidine latex particles neutralized with adsorbed PSS at IEP. Solid lines are results of the patch–charge model. Dependencies on the ionic strengths for molecular mass of 2260 kg/mol (left) and on the molecular mass at an ionic strength of 0.1 mM (right). (a) Decay length and (b) amplitude. The gray area indicates the regime between CC and CP boundary conditions.

roughness of 0.4 nm. The finite thickness of the adsorbed PSS layer is probably negligible, since a value of about 0.2 nm was found in a similar system by light scattering.¹⁵ Van der Waals forces could be equally interpreted without any displacement ($\delta = 0$), but a Hamaker constant of about factor 2–3 smaller than the expected one has to be adopted. Such small Hamaker constants were found with direct force measurements for cellulose⁴¹ and silica.⁴² Since the reported value of the Hamaker was confirmed independently, we think that the interpretation in terms of the displacement of the plane of origin is more appropriate.

The observed additional attractive non-DLVO forces are fully consistent with an exponential law. The dependence of the decay length and the amplitude are shown in Figure 8. The observed forces for PSS of molecular mass of 2260 kg/mol lead to a decay length of $q^{-1} = 2.4 \pm 0.1$ nm, which is independent of the ionic strength. On the other hand, the amplitude A decreases with increasing ionic strength rapidly. However, with decreasing molecular mass of PSS, the decay length and the corresponding amplitude decrease.

Electrostatic Patch–Charge Interactions. The additional exponential non-DLVO attraction is consistent with the patch–charge model. The present data were compared with the attractive forces expected from the electrostatic interaction between two identical surfaces with an inhomogeneous charge distribution arranged on a square lattice.³¹ This model predicts an exponential attraction with a decay length q^{-1} . This decay length is given by

$$q^2 = \kappa^2 + (\pi/a)^2 \quad (5)$$

where κ^{-1} is the Debye length defined in eq 1 and $2a$ is the lattice constant of the square lattice. This relation is consistent with the data in Figure 8a with a lattice constant of $2a \approx 15$ nm. Clearly, the adsorbed PSS does not form a regular lattice on the surface, but the size of surface heterogeneities visible in the AFM image is certainly comparable with the lattice constant estimated here. The molecular mass dependence was estimated

by assuming that $a \propto \Gamma^{-1/2}$. Figure 6 illustrates that the adsorbed mass at IEP is independent of the molecular mass M , and therefore we have $a \propto M^{1/2}$. This relation is shown in Figure 8, and indeed explains the observed trend quite well.

The amplitude depends on the boundary conditions. We have simplified the reported expressions for CC and CP for one small single patch within the unit cell.³¹ For CC conditions, one finds

$$A \approx \frac{4\pi\Delta\sigma^2\theta^2}{\epsilon_0\epsilon q} \quad (\text{CC}) \quad (6)$$

where $\Delta\sigma = \sigma_1 - \sigma_0$ is the difference between the surface charge density of the patch σ_1 and the surface density of the bare surface σ_0 and θ is the coverage of the small patches. For CP conditions, one obtains

$$A \approx \frac{4\pi q\Delta\sigma^2\theta^2}{\epsilon_0\epsilon k^2} \quad (\text{CP}) \quad (7)$$

These amplitudes are calculated as follows. At the IEP, one has $\sigma = 0$ in eq 3, and the difference in the charge density can be thus expressed as $\Delta\sigma = -\sigma_0(1 + 1/\theta)$. The coverage of $\theta \approx 0.35$ is found from the AFM image shown in Figure 2b. With the surface charge density of the bare surface of $\sigma_0 \approx 5.9$ mC/m², one finds $\Delta\sigma \approx -22$ mC/m². The predictions of this model are shown in the bottom part of Figure 8b, and they reflect similar trends as observed in the experimental data. The dependence on the molecular mass M is estimated by assuming a constant value of $\Delta\sigma$. The gyration radius R_g of PSS increases with the molecular mass as $R_g \propto M^\nu$ where $\nu \approx 0.6$ as for good solvent conditions.⁴³ This dependence suggests that the coverage increases slightly with the molecular mass, namely as $\theta \propto M^{2\nu-1}$.

While this patch–charge model is highly simplified, it semiquantitatively reproduces overall trends observed for the additional attractive force. While the decay length appears consistent with the model, we are currently unable to predict this quantity from the structure of the adsorbed layer. The experimentally observed amplitude is typically closer to the CC conditions, which represent the weakest forces predicted by the model. Nevertheless, regulation effects could be relevant in determining interactions between heterogeneously charged surfaces. The size of the interacting areas on the two particles may equally represent an important parameter. While these questions require further investigation, the overall agreement between the experimental data and the patch–charge model indicates that this model captures the basic mechanism of the observed attractive forces.

Conclusions

PSS adsorbs strongly to amidine latex particles and leads to charge reversal at the IEP. The interaction forces were studied with an AFM-based multiparticle colloidal probe technique and found to be mainly of electrostatic origin. Away from the IEP, forces are repulsive at larger separations and dictated by the overlap of diffuse layers. The strength of these forces can be rationalized with effective charges of the particle and of the PSS. The latter is about 2% of the bare charge of the polymer.

At shorter distances, and especially near the IEP, the interactions are dominated by exponential attractive forces with a range of 1–2 nm. These forces originate from the electrostatic interactions between the surface charge heterogeneities resulting from PSS adsorption to the oppositely charged latex. These

observations can be rationalized with a patch–charge model semiquantitatively.

Acknowledgment. Financial support was provided by the Swiss National Science Foundation, University of Geneva, Swiss Federal Office for Education and Science, and COST Action D43.

References and Notes

- (1) Perret, D.; Gaillard, J. F.; Dominik, J.; Atteia, O. *Environ. Sci. Technol.* **2000**, *34*, 3540–3546.
- (2) Grolimund, D.; Borkovec, M. *J. Contam. Hydrol.* **2006**, *87*, 155–175.
- (3) *Retention Aids*, 2nd ed.; Horn, D., Linhart, F., Eds.; Blackie Academic and Professional: London, 1996.
- (4) Bolto, B.; Gregory, J. *Water Res.* **2007**, *41*, 2301–2324.
- (5) de Gennes, P. G. *Nature* **2001**, *412*, 385–385.
- (6) Russel, W. B.; Saville, D. A.; Schowalter, W. R. *Colloidal Dispersions*; Cambridge University Press: Cambridge, U.K., 1989.
- (7) Chen, K. L.; Mylon, S. E.; Elimelech, M. *Langmuir* **2007**, *23*, 5920–5928.
- (8) Liu, A.; Wu, R. C.; Eschenazi, E.; Papadopoulos, K. *Colloids Surf., A* **2000**, *174*, 245–252.
- (9) Saito, T.; Koopal, L. K.; van Riemsdijk, W. H.; Nagasaki, S.; Tanaka, S. *Langmuir* **2004**, *20*, 689–700.
- (10) Gregory, J. *J. Colloid Interface Sci.* **1973**, *42*, 448–456.
- (11) Bauer, D.; Buchhammer, H.; Fuchs, A.; Jaeger, W.; Killmann, E.; Lunkwitz, K.; Rehmet, R.; Schwarz, S. *Colloids Surf. A* **1999**, *156*, 291–305.
- (12) Bouyer, F.; Robben, A.; Yu, W. L.; Borkovec, M. *Langmuir* **2001**, *17*, 5225–5231.
- (13) Lin, W.; Galletto, P.; Borkovec, M. *Langmuir* **2004**, *20*, 7465–7473.
- (14) Kleemann, J.; Gehin-Delval, C.; Auweter, H.; Borkovec, M. *Langmuir* **2005**, *21*, 3688–3698.
- (15) Gillies, G.; Lin, W.; Borkovec, M. *J. Phys. Chem. B* **2007**, *111*, 8626–8633.
- (16) Borkovec, M.; Papastavrou, G. *Curr. Opin. Colloid Interface Sci.* **2008**, *13*, 429–437.
- (17) Salmi, J.; Osterberg, M.; Stenius, P.; Laine, J. *Nord. Pulp Pap. Res. J.* **2007**, *22*, 249–257.
- (18) Poptoshev, E.; Rutland, M. W.; Claesson, P. M. *Langmuir* **1999**, *15*, 7789–7794.
- (19) Leong, Y. K.; Scales, P. J.; Healy, T. W.; Boger, D. V. *Colloids Surf., A* **1995**, *95*, 43–52.
- (20) Zhou, Y.; Gan, Y.; Wanless, E. J.; Jameson, G. J.; Franks, G. V. *Langmuir* **2008**, *24*, 10920–10928.
- (21) Dahlgren, M. A. G.; Waltermo, A.; Blomberg, E.; Claesson, P. M.; Sjostrom, L.; Akesson, T.; Jonsson, B. *J. Phys. Chem.* **1993**, *97*, 11769–11775.
- (22) Tadmor, R.; Hernandez-Zapata, E.; Chen, N.; Pincus, P.; Israelachvili, J. N. *Macromolecules* **2002**, *35*, 2380–2388.
- (23) Kirwan, L. J.; Maroni, P.; Behrens, S. H.; Papastavrou, G.; Borkovec, M. *J. Phys. Chem. B* **2008**, *112*, 14609–14619.
- (24) Block, S.; Helm, C. A. *Phys. Rev. E* **2007**, *76*, 030801.
- (25) Biggs, S.; Healy, T. W. *J. Chem. Soc., Faraday Trans.* **1994**, *90*, 3415–3421.
- (26) Biggs, S.; Dagastine, R. R.; Prieve, D. C. *J. Phys. Chem. B* **2002**, *106*, 11557–11564.
- (27) Elmahdy, M. M.; Synytska, A.; Drechsler, A.; Gutsche, C.; Uhlmann, P.; Stamm, M.; Kremer, F. *Macromolecules* **2009**, *42*, 9096–9102.
- (28) Popa, I.; Gillies, G.; Papastavrou, G.; Borkovec, M. *J. Phys. Chem. B* **2009**, *113*, 8458–8461.
- (29) Popa, I.; Papastavrou, G.; Borkovec, M.; Trulsson, M.; Jonsson, B. *Langmuir* **2009**, *25*, 12435–12438.
- (30) Richmond, P. *J. Chem. Soc., Faraday Trans. 2* **1975**, *71*, 1154–1163.
- (31) Miklavic, S. J.; Chan, D. Y. C.; White, L. R.; Healy, T. W. *J. Phys. Chem.* **1994**, *98*, 9022–9032.
- (32) O'Brien, R. W.; White, L. R. *J. Chem. Soc., Faraday Trans. 2* **1978**, *74*, 1607–1626.
- (33) Sader, J. E.; Larson, I.; Mulvaney, P.; White, L. R. *Rev. Sci. Instrum.* **1995**, *66*, 3789–3798.
- (34) Cleveland, J. P.; Manne, S.; Bocek, D.; Hansma, P. K. *Rev. Sci. Instrum.* **1993**, *64*, 403–405.
- (35) Hutter, J. L.; Bechhoefer, J. *Rev. Sci. Instrum.* **1993**, *64*, 1868–1873.
- (36) Pericot-Camara, R.; Papastavrou, G.; Behrens, S. H.; Borkovec, M. *J. Phys. Chem. B* **2004**, *108*, 19467–19475.
- (37) Borkovec, M.; Behrens, S. H. *J. Phys. Chem. B* **2008**, *112*, 10795–10799.
- (38) Pericot-Camara, R.; Papastavrou, G.; Borkovec, M. *Macromolecules* **2009**, *42*, 1749–1758.
- (39) Popa, I.; Papastavrou, G.; Borkovec, M. *Macromolecules* **2010**, *43*, 1129–1136.
- (40) Bevan, M. A.; Prieve, D. C. *Langmuir* **1999**, *15*, 7925–7936.
- (41) Notley, S. M.; Pettersson, B.; Wagberg, L. *J. Am. Chem. Soc.* **2004**, *126*, 13930–13931.
- (42) Dishon, M.; Zohar, O.; Sivan, U. *Langmuir* **2009**, *25*, 2831–2836.
- (43) Tanahatoe, J. J.; Kuil, M. E. *J. Phys. Chem. A* **1997**, *101*, 8389–8394.

JP911482A